Feature Space Optimization for Virtual Chromoendoscopy Augmented by Topography

Germán González[1], Vicente Parot[1], William Lo[2],
Benjamin J. Vakoc[2], and Nicholas J. Durr[1,*]

[1] Madrid-MIT M+Vision Consortium,
Massachusetts Institute of Technology, Cambridge MA 02139, USA
{ggonzale,vparot,ndurr}@mit.edu
[2] Wellman Center for Photomedicine, Harvard Medical School and
Massachusetts General Hospital, Boston MA 02114, USA
william_lo@hms.harvard.edu, vakoc.benjamin@mgh.harvard.edu

Abstract. Optical colonoscopy is the preferred modality for the screening and prevention of colorectal cancer. Chromoendoscopy can increase lesion detection rate by highlighting tissue topography with a colored dye, but is too time-consuming to be adopted in routine colonoscopy screening. We developed a fast and dye-free technique that generates virtual chromoendoscopy images that incorporate topography features acquired from photometric stereo endoscopy. We demonstrate that virtual chromoendoscopy augmented by topography achieves similar image quality to conventional chromoendoscopy in ex-vivo swine colon.

Keywords: optical colonoscopy, chromoendoscopy, photometric stereo endoscopy, topography.

1 Introduction

Colonoscopy screening reduces the risk of mortality from colorectal cancer by finding and removing precancerous lesions in the large intestine. However, the protective value of colonoscopy screening is limited because endoscopists frequently miss lesions [1, 2]. Chromoendoscopy is a technique that enhances tissue contrast in endoscopy by spraying and rinsing a dye over a tissue surface. Indigo carmine is often used as a chromoendoscopy dye for colonoscopy. As a nonabsorbed dye, indigo carmine increases lesion contrast by highlighting topographical irregularities in the colon mucosa [3]. Unfortunately, even though chromoendoscopy with indigo carmine is known to significantly improve adenoma detection rates [4, 5], it is not used in routine colonoscopy screening because the process of iteratively spraying and rinsing the dye dramatically increases the procedure timbale [1]. Thus there is a need for alternative techniques that increase the contrast from topographical features of the mucosa without increasing procedure time [6].
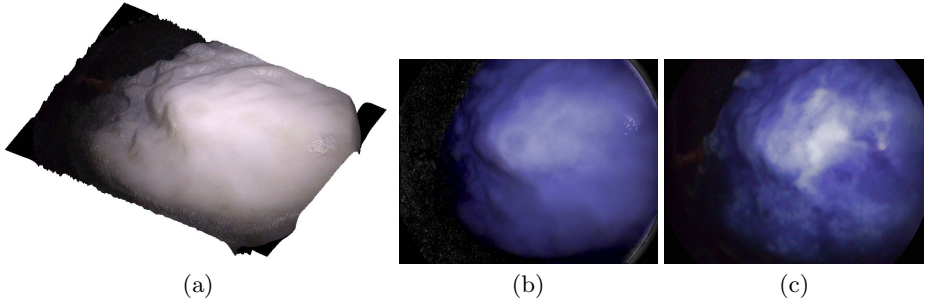

Fig. 1. (a) Image and topography obtained by PSE. (b) Virtual chromoendoscopy calculated by incorporating features from the image and topography of the same field of view as in (a). (c) Dye-based chromoendoscopy image performed in the same field of view as (a).

There have been several efforts to develop dye-free techniques for rapid virtual chromoendoscopy that would be practical for use in routine colonoscopy screening. For instance, Olympus, Pentax, and Fujinon have introduced Narrow Band Imaging (NBI), i-Scan, and Fujinon intelligent chromoendoscopy (FICE), respectively, as spectral approaches to emphasize superficial tissue structure and vascular patterns. All of these techniques create a non-photorealistic image using a combination of selected wavelength channels [7]. However, unlike dye-based chromoendoscopy, these virtual chromoendoscopy techniques have failed to show a convincing improvement in colonoscopy adenoma detection rates [8–10]. A major limitation of existing virtual chromoendoscopy approaches is that the origin of the contrast in these techniques (the optical properties of the tissue) is fundamentally different than that of dye-based chromoendoscopy (the tissue topography).

In this paper, we present a virtual chromoendoscopy technique that, unlike previous approaches, enhances contrast based on topographical features. We use photometric stereo endoscopy (PSE) [11], to acquire both the conventional uniform illumination images and high-frequency topographical images of the field-of-view. Though the low-frequency spatial information is not captured with PSE, the high-frequency topography is more clinically relevant. In fact, dye-based chromoendoscopy also preferentially highlights the sharp topographical changes in the mucosa surface. Our approach, called Virtual Chromoendoscopy Augmented with Topography (VCAT), produces images that are comparable to those obtained with dye-based chromoendoscopy (Figure 1).

2   Experimental Setup

Videos of tissue illuminated from a sequence of four alternating white-light sources were acquired using a Pentax gastroscope (EG-2990i) that was modified for clinical PSE in a similar manner to a previous report [12]. We used a Pentax

EPK-i5010 video processor which outputs a digital signal that is synchronized with the 15 Hz frame rate of the endoscope image sensor. The synchronization pulses were converted to a cycle of four sequential pulse trains that were sent to an LED driver via an Arduino microcontroller. The LEDs (Mightex FCS-0000-000) were coupled to 1mm light guides with diffusing tips at the distal end. We turned off the conventional light sources and used only these custom LED sources to illuminate the sample. The four optical fibers were oriented at equal angles about the center of the gastroscope tip. Each fiber delivered a maximum radiant flux of 18 mW of white light. The resulting system acquired high-definition images (1230 x 971 pixels) and enabled topographical reconstructions every four frames (3.75 Hz) in a system that has the same outer diameter (14 mm) as conventionally-used colonoscopes.

The high frequency topography of the field of view was calculated using a photometric stereo endoscopy method which reduces errors arising from an unknown working distance by assuming constant source vector directions and high-pass filtering the calculated topography map (11). The underlying assumption is that the error incurred in the fixed estimation of light source positions changes slowly from pixel to pixel, and can thus be corrected by filtering the shape gradients with a spatial frequency high-pass filter. The four source vectors for all pixels in the image were assumed to be equal to that of a pixel in the center of the field-of-view, for which source vectors were calculated assuming a 40 mm working distance. The resulting x and y gradients calculated by photometric stereo were high-pass filtered by subtracting a low-pass image resulting from blurring gradients with a 100 pixel Gaussian kernel with $\sigma = 100$ pixels. A height map is estimated from the high-pass filtered gradients using a multigrid solver for the Poisson equation that minimizes integration errors (11).

To demonstrate and validate the potential of topography-based virtual chromoendoscopy, we imaged three ex-vivo swine colons. Each of them was cleaned, cut, and spread open on a flat surface. The PSE endoscope was fixed above the tissue and images were acquired before and after spraying and rinsing an approximately 0.5% solution of indigo carmine chromoendoscopy dye. Although there are no accessible swine models for colorectal cancer, swine colon do exhibit a range of surface topographies that are qualitatively similar to normal and abnormal regions in the human colon.

3 Virtual Chromoendoscopy Augmented with Topography

We use PSE to simultaneously acquire conventional white light images and topography information. Specifically, we calculate the uniformly illuminated image I_u, the surface normal maps $\mathbf{N}$, and the tissue height maps h from the PSE images. VCAT combines information from the conventional, uniformly-illuminated image and topographical measurement to emulate the dye accumulation in topographical features in dye-based chromoendoscopy (Algorithm 1).

Data: Photometric Stereo Images **I**. Weight vector w
Result: Virtual Chromoendoscopy Image I_{VCAT}
while *New Image I_n* **do**
  – remove specular reflections from $I_n \rightarrow I_n^c$
  – perform PSE to compute the normal and height maps
     $\mathbf{I}^c = \{I_n^c, I_{n-1}^c, I_{n-2}^c, I_{n-3}^c\} \rightarrow \{h, \mathbf{N}\}$
  – estimate a uniformly illuminated image from $\mathbf{I}^c \rightarrow I_u$
  – equalize the image to match the color and intensity properties of a canonical
     chromoendoscopy image $I_u \rightarrow I_e$
  – generate features from $\{I_e, h, \ \mathbf{N} \ \} \rightarrow \mathbf{f}$
  – combine the features to generate the VCAT image $I_{VCAT} = f(\mathbf{f})$

end

Algorithm 1. Virtual chromoendoscopy augmented with topography

3.1   Removal of Specular Reflections

We use a photometric stereo algorithm that assumes that the object has a Lambertian surface remittance. Consequently, specular reflections from the wet tissue surface create artifacts in the topographical reconstruction. These errors create artificial dips and bumps that may be highlighted by virtual chromoendoscopy. Since the fiber optics of our photometric stereo system closely represent point sources and the surface of the colon varies smoothly, specular reflections appear in our images as circular-like shapes of high brightness. To detect them we use a scale-space approach based on the Laplacian of a Gaussian filter. For each image I_n we compute its convolution with a Laplacian of Gaussian filters at different scales σ and normalize them with σ^2. We then project the scale-space approach into a single 2-dimensional image $I_L = \max_\sigma (I_n * LoG_\sigma)\sigma^2$. Pixels that have a greater value than the mean plus three standard deviations in I_L are considered specular reflections and removed from the image. The values of the corrected image I_n^c at those locations are estimated by solving Laplace's equations from its boundary pixels.

3.2   Features for computing VCAT

For each set of images **I**, we compute features that are combined to generate a virtual chromoendoscopy luminance image. We compute five features that are based on both the image information as well as the topography:

Equalized uniformly illuminated image I_e: We compute I_e as the L channel of the mean value of the four sequential images acquired by the PSE system, after correcting for specular reflections and converting it into Lab color space. $\bar{I} = (I_n^c + I_{n-1}^c + I_{n-2}^c + I_{n-3}^c)/4$. We adjust the brightness and contrast of the uniformly illuminated image so that it matches those of a canonical chromoendoscopy image.

Height map: We decompose the height map obtained from PSE into two features: **pits** and **crevices**, depending on whether the height map is positive or negative.

θ: Angle of the surface normal with respect to the z direction.

Image offset: A vector of ones added to compensate for image offsets.

3.3   Feature Combination

The goal of virtual chromoendoscopy is to replicate as faithfully as possible an objective chromoendoscopy image I_{ch}. Towards that end, we estimate the luminance of the VCAT image as a linear combination of image and topological features $\mathbf{f}$. We use a minimization process to obtain the weight vector $\hat{w}$ that optimally combines the features, using as a cost function the squared error between the estimated luminance image and the luminance of the real chromoendoscopy image I_{ch}^{L},

$$\hat{w} = \underset{w}{\operatorname{argmin}} ||I_{ch}^{L} - \mathbf{f} \cdot w||. \tag{1}$$

This linear problem can be solved by applying Moose-Penrose pseudoinversion of the feature matrix and multiplying it by the objective image:

$$\hat{w} = pinv(\mathbf{f}) \cdot I_{ch}^{L}. \tag{2}$$

The same process can be applied when estimating the weighting vector $\hat{w}$ with several images by changing the objective image I_{ch} and the features $\mathbf{f}$ in Eq. 1 for a concatenation of the images and features.

3.4   Virtual Chromoendoscopy Image Estimation

Given an input image I_n, its features $\mathbf{f}$, and the weight vector computed previously $\hat{w}$, the luminance of the virtual chromoendoscopy image I_{VCAT}^{L} is estimated as a linear combination of the features, using as weights $\hat{w}$:

$$I_{VCAT}^{L} = \mathbf{f} \cdot \hat{w}. \tag{3}$$

The color components of the virtual chromoendoscopy image are obtained by equalizing the chrominance of the original image I_n to match the chrominance of the canonical chromoendoscopy image.

4   Evaluation

We equalized the brightness and contrast of each I_{ch} acquired in three different swine colons to reduce illumination artifacts. We evaluated the VCAT by comparing I_{VCAT}^{i} with I_{ch}^{i}.
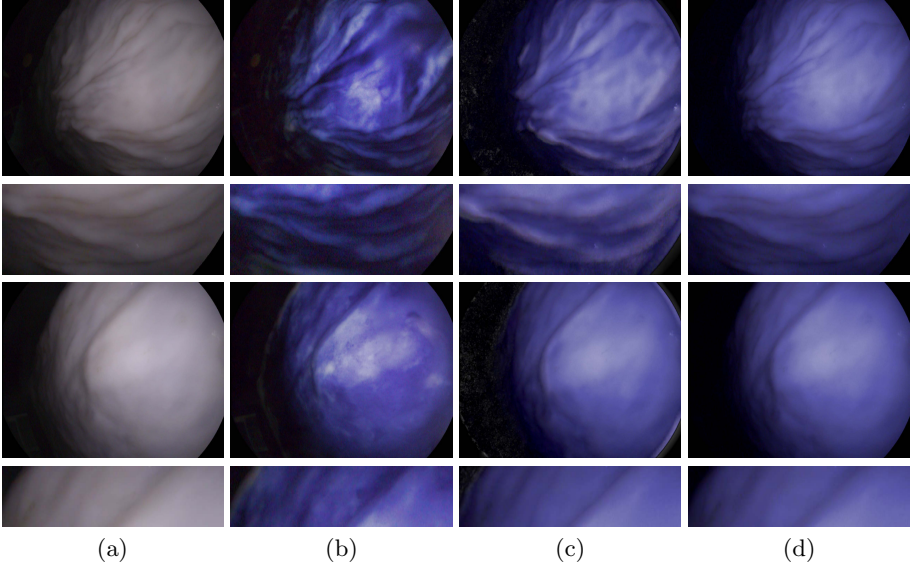
Fig. 2. First and third samples of our training images. Second and fourth rows show zoomed in regions of the samples. (a) Original images after removing specular reflections. (b) Image of same field of view as left column after applying dye-based chromoendoscopy. (c) VCAT. (d) Virtual chromoendoscopy by equalizing the color statistics of the conventional image in the left column to that of the chromoendoscopy image in the middle-left column. Qualitatively, the VCAT technique appears to enhance regions with ridges in the same way that real chromoendoscopy does, as highlighted in the second and fourth rows.

4.1   Evaluation Methodology

We performed leave-one-out cross-validation to estimate the performance of the system on unseen images. For each image sample i, we compute the weighting vector $\hat{w}_i$ with the remaining pair of PSE images and real chromoendoscopy and reconstruct the estimated I_{VCAT}^i.

In order to evaluate if the topographical features described in Section 3.2 help on the generation of realistic VCAT images, we generate virtual chromoendoscopy images without using the topographical features: I_{vc}^i. We do so by adjusting the brightness, contrast and color channels of the uniformly illuminated images to that of the canonical chromoendoscopy image. We compare those two sets of virtual chromoendoscopy images, $\{I_{VCAT}^i\}$ and $\{I_{vc}^i\}$, to the objective image, $\{I_{ch}^i\}$, using two similarity measurements: root mean squared error (RMSE) and the structural similarity index (SSIM) [13]. The SSIM index is a framework for image comparison as a function of their luminance, contrast, and structural similarity. Since we are minimizing the norm of the difference between $\{I_{VCAT}^i\}$ and $\{I_{ch}^i\}$, the RMSE will correspondingly decrease within the training set. However, since we are performing leave-one-out cross-validation the RMSE from the test image is a valid metric for evaluation.

Table 1. Quantification of the similarity between real chromoendoscopy, the proposed virtual chromoendoscopy, and virtual chromoendoscopy by color equalization for the two evaluation metrics: RMSE and SSIM

Measure	RMSE				SSIM			
Sample	S1	S2	S3	p-value	S1	S2	S3	p-value
I_{VCAT}	3.06	6.32	4.12	0.08	0.882	0.747	0.848	0.026
I_{vc}	3.21	6.68	4.28		0.815	0.704	0.771	

We further demonstrate our system in three different videos of the porcine colon. However, we can not quantify the effects of virtual chromoendoscopy in such videos since we do not have registered real chromoendoscopy frames to them.

5   Results

Figures 1 and 2 compare images obtained from VCAT and real chromoendoscopy. As expected, images from VCAT incorporate topographical contrast by highlighting the ridges and darkening the pits in the colon mucosa. Figure 2 also shows virtual chromoendoscopy obtained by color equalization. Color equalization is done by scaling and shifting the a and b components of the image in *Lab* color space to match those of a canonical chromoendoscopy image. Qualitatively, VCAT produces images that are more similar to real chromoendoscopy than virtual chromoendoscopy by color equalization, as highlighted in the second and fourth rows of Fig. 2.

The quantification of the image improvement is shown in Table 1. Incorporating topographical features results in both lower RMSE and higher SSIM. We performed a student t-test on the results to show their statistical significance. Although we have only three points in our dataset, the improvement p-value for the SSIM metric is statistically significant.

6   Discussion

While PSE can reconstruct the 3D topography of the colon surface, the interpretation of this additional information may require a steep learning curve for the gastroenterologist. Chromoendoscopy, on the other hand, highlights features from the colon topography in a way that is intuitive and familiar to gastroenterologists. In this paper we have proposed a method to generate images that are similar to chromoendoscopy but incorporate the 3D topography of the field of view that is easily and quickly acquired from PSE. We have showcased and quantified the technology in a dataset of three registered images of three ex-vivo swine colon, demonstrating that virtual chromoendoscopy images that include topographical information more closely resemble real chromoendoscopy images than those that do not include topographical information. This technique could enable

gastroenterologists improve their lesion detection rates in routine colonoscopy by incorporating the clinically-valuable topographical contrast obtained by PSE in a familiar representation. The evaluation of the performance of VCAT in ex-vivo and in-vivo human colon tissue is underway.

References

1. Rex, D.K.: Maximizing detection of adenomas and cancers during colonoscopy. The American Journal of Gastroenterology 101(12), 2866–2877 (2006)
2. Pohl, H., Robertson, D.J.: Colorectal cancers detected after colonoscopy frequently result from missed lesions. Clinical Gastroenterology and Hepatology: the Official Clinical Practice Journal of the American Gastroenterological Association 8(10), 858–864 (2010), PMID: 20655393
3. Song, L.M.W.K., Adler, D.G., Chand, B., Conway, J.D., Croffie, J.M.B., DiSario, J.A., Mishkin, D.S., Shah, R.J., Somogyi, L., Tierney, W.M., Petersen, B.T.: Chromoendoscopy. Gastrointestinal Endoscopy 66(4), 639–649 (2007)
4. Brooker, J.C., Saunders, B.P., Shah, S.G., Thapar, C.J., Thomas, H.J.W., Atkin, W.S., Cardwell, C.R., Williams, C.B.: Total colonic dye-spray increases the detection of diminutive adenomas during routine colonoscopy: A randomized controlled trial. Gastrointestinal Endoscopy 56(3), 333–338 (2002)
5. Hurlstone, D.P., Cross, S.S., Slater, R., Sanders, D.S., Brown, S.: Detecting diminutive colorectal lesions at colonoscopy: a randomised controlled trial of pan-colonic versus targeted chromoscopy. Gut 53(3), 376–380 (2004), PMID: 14960519
6. Durr, N.J., Gonzlez, G., Parot, V.: 3D imaging techniques for improved colonoscopy. Expert Review of Medical Devices 11(2), 105–107 (2014), PMID: 24387658
7. Pohl, J., May, A., Rabenstein, T., Pech, O., Ell, C.: Computed virtual chromoendoscopy: a new tool for enhancing tissue surface structures. Endoscopy 39(1), 80–83 (2007), PMID: 17252465
8. Adler, A., Pohl, H., Papanikolaou, I.S., Abou-Rebyeh, H., Schachschal, G., Veltzke-Schlieker, W., Khalifa, A.C., Setka, E., Koch, M., Wiedenmann, B., Rösch, T.: A prospective randomised study on narrow-band imaging versus conventional colonoscopy for adenoma detection: does narrow-band imaging induce a learning effect? Gut 57(1), 59–64 (2008), PMID: 17681999
9. Nass, J.P., Connolly, S.E.: Current status of chromoendoscopy and narrow band imaging in colonoscopy. Clinics in Colon and Rectal Surgery 23(1), 21–30 (2010), PMID: 21286287 PMCID: PMC2850163
10. Rex, D.K., Helbig, C.C.: High yields of small and flat adenomas with high-definition colonoscopes using either white light or narrow band imaging. Gastroenterology 133(1), 42–47 (2007), PMID: 17631129
11. Parot, V., Lim, D., Gonzlez, G., Traverso, G., Nishioka, N.S., Vakoc, B.J., Durr, N.J.: Photometric stereo endoscopy. Journal of Biomedical Optics 18(7), 076017–1–076017–7 (2013), PMID: 23864015
12. Durr, N.J., Gonzalez, G., Lim, D., Traverso, G., Nishioka, N.S., Vakoc, B.J., Parot, V.: System for clinical photometric stereo endoscopy. In: Advanced Biomedical and Clinical Diagnostic and Surgical Guidance Systems XII, San Francisco, CA, vol. 8935(51). SPIE (February 2014)
13. Wang, Z., Bovik, A.C., Sheikh, H.R., Simoncelli, E.P.: Image quality assessment: from error visibility to structural similarity. IEEE Transactions on Image Processing 13(4), 600–612 (2004)